

Generalized Formulation to Predict Rossiter Modes for Subsonic to Hypersonic Flow

Jeremy P. Redding^{1,2,3}, Luis Bravo³, Prashant Khare^{1,2}

¹Department of Aerospace Engineering, University of Cincinnati, Cincinnati, OH 45221-0070, USA

²Hypersonics Laboratory, Digital Futures, University of Cincinnati, Cincinnati, OH 45206, USA

³DEVCOM Army Research Laboratory, Army Research Directorate, Aberdeen Proving Ground, MD 21005, USA

Abstract. This paper describes the development of a generalized physics-based model to accurately estimate Rossiter modes for flow over rectangular cavities for regimes ranging from subsonic to hypersonic without the a priori knowledge of flow physics. The Heller-Bliss model is shown to diverge from direct numerical simulation (DNS) results, while the adapted model shows close alignment (within 10%) with the DNS data at higher Mach numbers, and is physically reasoned on the basis of energy modes. Using an effective temperature to evaluate the speed of sound calculations and then using it to calculate the Strouhal number yields closer predictions to DNS data. The present work also establishes asymptotic limits for Strouhal numbers.

1 Introduction

When a flow passes over a rectangular cavity, a shear layer develops due to the velocity and density differences between the freestream and the fluid inside the cavity. This shear layer is a zone of intense vorticity and is characterized by both a shedding frequency and a frequency associated with its impingement on the cavity's trailing wall. The latter phenomenon (impingement on the trailing wall) generates pressure waves that propagate upstream, often as acoustic waves, which enhance separation at the leading-edge shear layer. The induced pressure gradient deflects the shear layer upward, while the freestream acts against this deflection, driving the shear layer back down to re-impinge on the trailing wall again. This sequence repeats, forming a self-sustaining oscillatory cycle. The excited modes from this process are referred to as Rossiter modes. In his seminal paper, Rossiter (1964) proposed an equation to predict the Strouhal number. The equation, as shown below, is based on thin-sheet oscillation theory with coefficients fitted using experimental data.

$$St = \frac{m - \alpha}{1/\kappa_v + M_\infty} \quad (1)$$

In this equation, the value m is the mode number, M_∞ is the freestream Mach number, and κ_v is the convective velocity, which is the relative weighted velocities between the free-stream and cavity. In cavity flows, typically one of the first two modes is amplified (see figure 7 in Rossiter (1964)). In Rossiter's work, pressure was measured at $x/L = 0.9$ on the lower wall of the cavity, which was then used to generate a frequency spectrum and subsequently, the peak frequency is utilized to predict Strouhal numbers. This form presented by Rossiter assumes subsonic freestream flow. Accounting for compressibility effects, Heller & Bliss (1975) modified equation 1 using Crocco's theorem as shown below:

$$St = \frac{m - \alpha}{M_\infty / \sqrt{1 + \frac{\gamma-1}{2} M_\infty^2} + 1/\kappa_v} \quad (2)$$

This form has been shown in the literature to accurately predict the Strouhal numbers for flows up to Mach ≈ 3 (Heller & Bliss (1975)). Recently, DeChant (2019) proposed a model to predict the Strouhal number

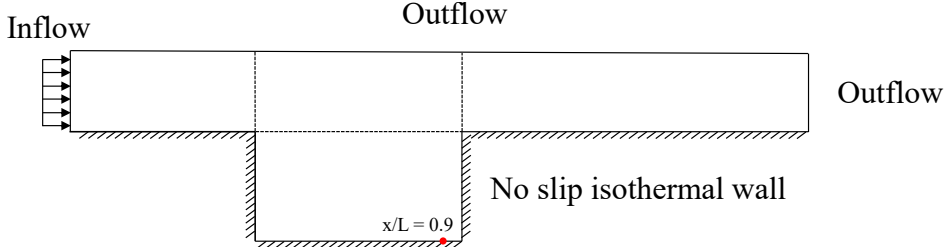


Figure 1: Schematic of the configuration. The pressure is measured at $x/L = 0.9$, similar to the study of Rossiter (1964).

that takes into account changes in cavity depth, creating the first ever depth-sensitized form of the equation. This equation has fewer coefficients and has a reasonable predictive capability up to $Mach \approx 3$. However, based on data from recent work on hypersonic flow over rectangular cavities (Redding *et al.*, 2023, 2025), this model diverges from observed Strouhal numbers for Mach numbers beyond 4.

In this manuscript, we generalize the analysis to encompass higher Mach numbers by introducing physically motivated modifications to the acoustic time-scale term in Rossiter's original formulation (see equation 1). After establishing the revised model, we evaluate its accuracy using data obtained from two-dimensional DNS simulations of thermochemical nonequilibrium hypersonic flow over a rectangular cavity, covering Mach numbers from 2 to 9. We note, as a caveat, that the use of 2D simulations prevents us from capturing vortex stretching; however, because the flow in this configuration is fundamentally two-dimensional and the simulations successfully reproduce the Strouhal numbers at lower Mach numbers reported in earlier studies, this choice is considered appropriate.

2 Numerical method and problem setup

The numerical simulations are based on the fully compressible form of Navier-Stokes equations with models to account for thermal and chemical nonequilibrium. These equations are solved using the open-source library, Eilmer (Gibbons *et al.* (2023)). Cases ranging from Mach 2 to 6 assumed ideal gas (i.e., no thermochemical nonequilibrium; results were identical when compared with simulations with non-equilibrium models switched on). For the cases at Mach 7 to 9, the 5 species non-equilibrium air model of Gupta *et al.* (1990) is used. For all cases, the initial composition of air in the freestream is assumed to be $N_2 = 0.767, O_2 = 0.233$. Time stepping is handled explicitly, with a third order Runge Kutta scheme. We use a fixed CFL number of 0.5, which leads to an average dt of 5.5×10^{-9} s.

Figure 1 presents a schematic of the setup, indicating the boundary conditions and the probe location. A DNS-level uniform grid is employed in both the x- and y-directions, meaning it is constructed to capture all relevant scales from the largest structures down to the Kolmogorov scale. As mentioned earlier, our simulations are two-dimensional; the absence of the vortex stretching term can moderately damp acoustic oscillations. Consequently, vortices are expected to survive longer in 2D computations. Additional information about the grid and boundary conditions is provided in our recent publication (Redding *et al.*, 2025). It should also be noted that the grid used in this study was originally optimized for Reynolds numbers associated with Mach 11, so for the lower Mach numbers examined here, the resulting grid resolution is highly conservative. The initial flow conditions consists of $M_\infty = [2, 3, 4, 5, 6, 7, 8, 9], T_\infty = 76$ K and $p_\infty = 19,330$ Pa. As shown in the figure, a probe is positioned on the cavity's lower wall at $x/L = 0.9$, identical to the location used by Rossiter (1964). In the present study, the dominant amplified mode corresponds to the second Rossiter mode; therefore, the mode number is taken as 2 in the analytical analysis presented in the following sections.

3 Generalized Rossiter Modes

3.1 Hypersonic Rossiter Modes

The dominant frequencies within a cavity are dependent on the geometry of the cavity, the Mach number in the flow M_∞ , and the Reynolds number of the flow. Fundamental frequencies in subsonic and transonic rectangular cavities based on Rossiter (1964) is given by:

$$f_m = \frac{U_\infty}{L} \left[\frac{m - \alpha}{M_\infty + 1/\kappa_v} \right] \quad (3)$$

As mentioned earlier, this equation was extended by Heller & Bliss (1975) to account for compressibility, and subsequently by DeChant (2019) to account for cavities with different L/D.

When we tested these models using our 2D DNS simulations, the model predictions agreed well, up to Mach numbers of 3, but they started to diverge for higher Mach numbers (results shown later in this section). Therefore, to develop a model that is valid for higher Mach numbers, we start our theoretical analysis from Euler's formula, according to which, the oscillatory behavior of cavity flow can be represented as:

$$e^{i\omega t} e^{i\varphi} = 1 \quad (4)$$

This is the equation for a closed feedback loop. In practice, though, cavity feedback does not behave as a completely closed system because of the mass outflow occurring near the trailing edge (Rockwell & Naudascher, 1978). In spite of this, it has been a good approximation thus far and will be used here. When we break down the time component of the feedback equation into two parts, an acoustic contribution and a shear layer contribution, the equation becomes:

$$e^{i\omega(\tau_a + \tau_c)} e^{i\varphi} = 1 \quad (5)$$

in order for the above to be true, then the following must also be true:

$$\omega(\tau_a + \tau_c) + \varphi = 2\pi n \quad (6)$$

If the convective time is L/U_c where L is the length of the cavity and U_c is the convective velocity, the above equation becomes:

$$\frac{\omega \left(\frac{L}{U_c} + \tau_a \right)}{2\pi} + \frac{\varphi}{2\pi} = n \quad (7)$$

Eventually, we define $f = \frac{\omega}{2\pi}$, $St = \frac{fL}{U_\infty}$ and $\alpha = \frac{\varphi}{2\pi}$ and substitute it in the above equation, it leads to:

$$St = \frac{n - \alpha}{\frac{U_c}{U_\infty} + \frac{U_\infty}{L} \tau_a} \quad (8)$$

Next, notice that U_c/U_∞ is the same as $1/\kappa$, and by applying the same assumption as Rossiter, that is, $\tau_a = L/a_\infty$, we recover the Rossiter equation:

$$St = \frac{n - \alpha}{\frac{1}{\kappa} + M_\infty} \quad (9)$$

Since α and κ appear to change very little in the literature, τ_a , the acoustic time scale, is likely the term that needs to be carefully assessed; an argument made by Heller & Bliss (1975) as they modified the original form to incorporate compressibility. Within the Heller-Bliss correction, Crocco's theorem shows some Mach number independence at around Mach 4. This also makes the Strouhal number approach independence at

the same Mach number. In Rossiter's formula, as the flow was subsonic both in the interior and exterior of the cavity, the assumption that the acoustic time scale (speed of sound) in the cavity being the same as the freestream was appropriate. The modifications of Heller & Bliss (1975) were based on the fact that the speed of sound inside and outside of the cavity is not the same.

For hypersonic flows, the speed of sound is also dependent on temperatures (vibrational, transrotational, and eventually electronic) and species concentrations, and cannot be estimated using $\sqrt{\gamma RT}$ with a constant temperature and gas constant.

Based on basic gas dynamic theory (Vincenti *et al.*, 1966), the speed of sound of an ideal dissociating gas for chemically frozen, a_f^2 and equilibrium, a_e^2 cases can be written as:

$$a_f^2 = \frac{RT(4 + \alpha)(1 + \alpha)}{3} \quad (10)$$

$$a_e^2 = \frac{RT\alpha(1 - \alpha)(1 + 2\tau) + (8 + 3\alpha - \alpha^3)\tau^2}{\alpha(1 - \alpha) + 3(2 - \alpha)\tau} \quad (11)$$

where $\tau = T/\theta$, θ is the dissociation temperature of the presumed diatomic molecule and T is the freestream temperature, which in this case is 76 K. We can take this simplification a step further for the sake of our asymptotic analysis and look at the limits based on α . The variable α is the "level of dissociation" of the gas, with $\alpha = 0$ corresponding to no dissociation and $\alpha = 1$ as fully dissociated.

The limits on the frozen speed of sound on the basis of chemical dissociation is then:

$$a_{f,L} = \sqrt{\frac{4}{3}RT} \leq a_f \leq a_{f,U} = \sqrt{\frac{10}{3}RT} \quad (12)$$

and the equilibrium equation limits are:

$$a_{e,L} = \sqrt{\frac{4}{3}RT\tau} \leq a_e \leq a_{e,U} = \sqrt{\frac{10}{3}RT\tau} \quad (13)$$

Substituting these limiting functions into the Strouhal equation in place of the usual freestream speed of sound, i.e., replacing τ_a with $L/a_{e,f}$ provides the asymptotes for the St number. [Table 1](#) lists the comparison between simulation results with frozen limits and the Heller-Bliss estimates.

Table 1: Comparison of Strouhal number from present DNS calculations with those of Heller & Bliss (1975) model. Also included are the chemically frozen limits obtained from equation 12. Red font indicates values out of the frozen bounds, and orange is nearly outside the bounds. Note, Mach 7 and above utilized non-equilibrium gas models in CFD

Case	Mach 2	Mach 4	Mach 6	Mach 7	Mach 8	Mach 9
Frozen lower limit ($St_{f,L}$)	0.484	0.40	0.23	0.203	0.18	0.16
St_{DNS}	0.56	0.45	0.38	0.28	0.32	0.29
$St_{Heller-Bliss}$	0.57	0.49	0.478	0.474	0.471	0.469
Frozen upper limit ($St_{f,U}$)	0.696	0.49	0.41	0.369	0.34	0.31

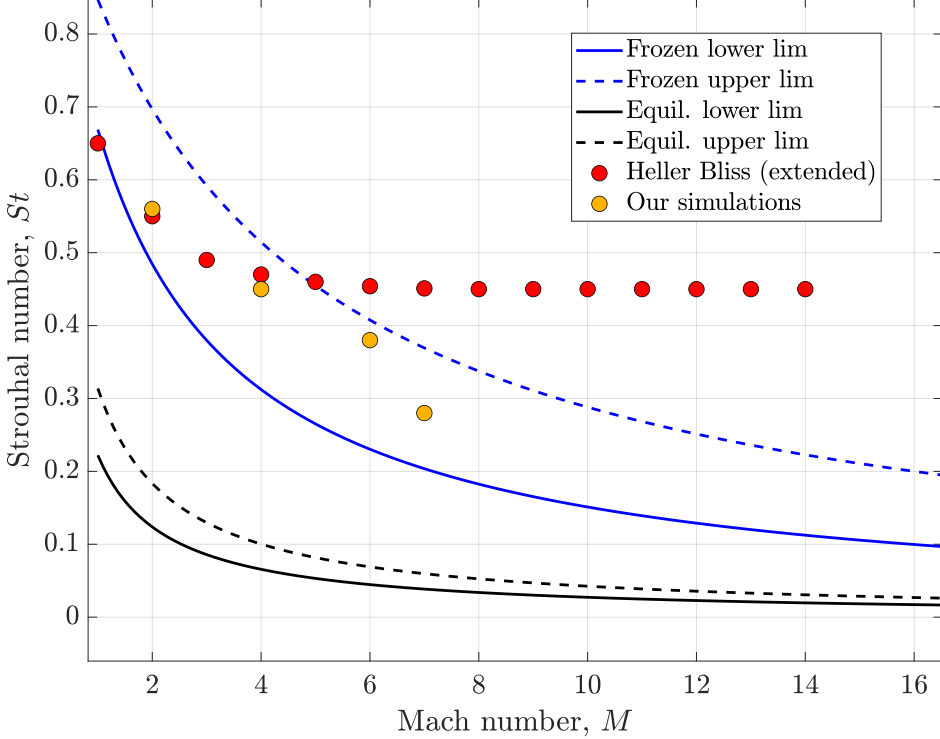


Figure 2: Mach number verses Strouhal number for present freestream temperature, extended to Mach 16

A few inferences can be made from Table 1. First, the Strouhal number at Mach 2 from DNS simulations agree well with Heller & Bliss (1975) model as this model is validated up to Mach 3. Second, as expected, there is a decreasing trend in Strouhal number as Mach number increases. This is where the similarities between DNS calculations and previous models end. Given that previous models assumed the gas to be non-reactive and calorically perfect, the Strouhal number should lie within the bounds of frozen and equilibrium flows. However, as the Mach number increases beyond 4, the Heller & Bliss (1975) estimate diverges from these bounds. On the other hand, our simulations, especially those up to Mach 6 where the air was assumed to be ideal, indicate that while St decreases, it stays in the aforementioned bounds. Further, to confirm our hypothesis, we conducted calculations for Mach numbers up to 6 while modeling nitrogen dissociation and found that the results did not change. This makes sense because at these Mach numbers, we do not expect much dissociation in the given configuration.

To investigate these limits further, we plot the frozen and equilibrium assumptions for our current freestream temperature verses Mach number. As shown in Figure 2, as Mach number increases, the Strouhal number function begins to approach a limit. Again, the equilibrium assumption approaches its asymptote much more quickly than that of the frozen assumption. It is important here to note the significant divergence between the Heller-Bliss model and the one predicted by employing a speed of sound found by the frozen assumption. While the Heller-Bliss asymptote is $St = 0.45$, the frozen flow limit does not occur until much higher in Mach number, and appears to be between 0.08 for the lower frozen limit and 0.15 for the upper frozen limit.

The next logical question to answer is the impact of temperature on Strouhal number. Although the previous models were good for low Mach numbers, they did not incorporate the effect of flow enthalpy, which becomes increasingly important as the Mach number increases. While the above asymptotic analysis showed that upper and lower limits of the Strouhal number, to obtain a more accurate prediction, we need to identify an appropriate temperature. To reiterate, the underlying concept of this analysis is to estimate

the Strouhal number without the knowledge of the actual conditions in the cavity. In the next section, we propose a physics-based model to identify an appropriate temperature based on distribution of energy in the various modes that are activated as Mach number increases.

3.2 Impact of energy distribution on Rossiter functions at high Mach numbers

As flow enters a supersonic or hypersonic cavity, the freestream flow passes through rapid compression at the leading edge due to the boundary layer impingement with the recirculating flow in the cavity. The rapid compression forms a shock, which is more deflected the further away from the boundary layer we observe, forming an oblique shock of different angles based on the Mach number and time instance of the oscillations in the cavity. Due to the unsteady behavior of this phenomena, accurately predicting the angle of the oblique shock is nearly impossible without conducting calulations or experiments. Instead, we can assume that since there is rapid compression at the leading edge, an appropriate assumption for the shock behavior closest to the boundary analytically is a normal shock.

From basic gas dynamics theory, the temperature across the normal shock (T_2) can easily be calculated using the freestream Mach number and temperature. T_2 represents the temperature just above the cavity and closest to the shear layer. As Mach number increases, T_2 increases, and at higher temperatures, other energy modes (in addition to translation) are populated. For simplicity, and knowing that standard air consists of 76% N_2 , the following analysis uses N_2 properties to estimate conditions. For Mach numbers of interest (up to 10), we expect energy to be distributed among translation, rotational and vibrational modes. The energy contained in these three modes can be estimated by:

$$U_{\text{trans}} = \frac{3}{2}RT_2, \quad U_{\text{rot}} = RT_2, \quad U_{\text{vib}} = \frac{R\theta_v}{e^{\theta_v/T_2} - 1}. \quad (14)$$

Note that these expressions must be modified based on the molecule of interest.

Since we intend to develop a model that can be used to estimate Rossiter modes using simple expressions, in the following paragraph we estimate an effective temperature that takes into account the energy distribution in various modes, which can then be substituted in the expression for speed of sound for a thermally perfect gas. In this context, we propose the following definition of an effective temperature:

$$T_{\text{eff}} = T_{\text{eff}}(U_{\text{trans}}, U_{\text{rot}}, U_{\text{vib}}) \quad (15)$$

where the dependent variables in T_{eff} are piecewise and dependent on Mach number regimes given by:

$$T_{\text{eff}}(M) = \begin{cases} T_2 & \text{for } M_\infty < 3 \\ T_2 \frac{U_{\text{trans}}}{U_{\text{total}}}, & \text{for } 3 < M_\infty < 5 \\ \left(T_2^2 \frac{U_{\text{trans}} U_{\text{rot}}}{U_{\text{total}}^2} \right)^{1/2} & \text{for } 5 < M_\infty < 7 \\ \left(T_2^3 \frac{U_{\text{trans}} U_{\text{rot}} U_{\text{vib}}}{U_{\text{total}}^3} \right)^{1/3} & \text{for } M_\infty \geq 7. \end{cases} \quad (16)$$

It is critical to restate that the effective temperatures described above does not represent an actual thermodynamic temperature for each mode. However, the fraction of energy allocated to translational, rotational, and vibrational degrees of freedom is closely linked to the activation of those modes and the resulting effective stiffness of the gas. The speed of sound relies on the slope of the pressure-density curve, which decreases as more energy is stored in internal modes. As internal energy modes become more active, the effective heat capacity increases and the gas becomes less stiff, reducing speed of sound. Thus, the

effective temperature, T_{eff} can be viewed as a surrogate parameter that reflects the Mach number and temperature dependence of internal degrees of freedom.

We propose to use T_{eff} , which serves as an empirical activation to calculate the speed of sound at different Mach numbers, given by:

$$a_{eff}(M_\infty) = \sqrt{\gamma R T_{eff}(M_\infty)} \quad (17)$$

[Figure 3](#) shows the resulting estimates of the Strouhal number using equation 17 in place of a_∞ in [Equation 8](#). The model performs quite well and captures the decreasing and increasing trends observed in the DNS calculations. Also shown in [Figure 3](#) is the Heller-Bliss model for reference. To further quantify the accuracy of the model, [Figure 2](#) shows the percentage error between the proposed model and DNS data. The estimates are within 10.3% of the values measured by DNS data. Using just the standard temperature or only one component of the temperature causes a significant divergence from the true value. As an example to highlight the importance of this finding, at Mach 7, if only T_{trans} is used to predict speed of sound, instead of the recommended piecewise function, the resulting Strouhal number is $St = 0.403$ which is a 43% difference.

4 Conclusion

A new model for computing Strouhal number based on freestream temperatures is presented. The Heller-Bliss model is shown to diverge from the CFD results, while the adapted model shows close alignment with the CFD results, and is physically reasoned on the basis of energy modes. Two methods are shown with increasing precision. As a first prediction approach, one could calculate the minimum and maximum speed of sound, and utilize this new value in the Strouhal number calculation to predict a minimum and maximum Strouhal value. This is a more rapid approach to determine "problem frequency ranges" of interest for the specific problem, and whether or not a finer approach is needed. Separately, for a better prediction, the second method can be employed. This method has four distinct regimes on the basis of temperatures and energy modes. Using these temperatures in the speed of sound calculations, the Strouhal equation yields closer predictions to the exact Strouhal number.

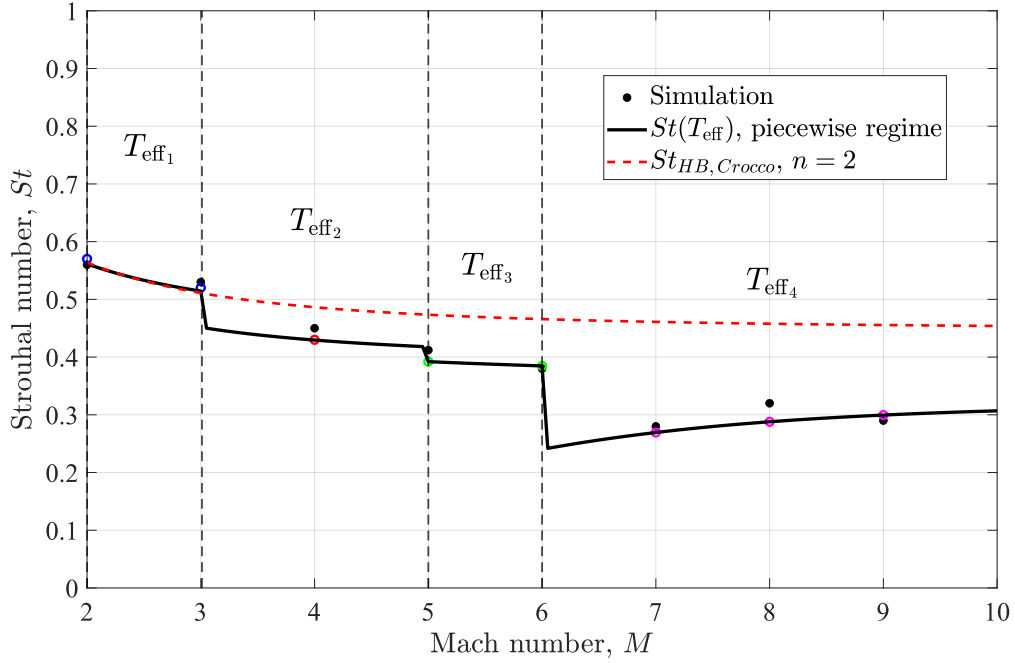


Figure 3: Regime diagram: Strouhal number vs Mach number, overlaid with DNS data. Also shown is the Heller-Bliss model.

Table 2: Comparison of CFD-estimated Strouhal number calculated using the pressure signal at $x/L = 0.9$, proposed model and Heller-Bliss predictions. Colored datapoints correspond to differentiated regimes in Figure 3.

Case	Mach 2	Mach 3	Mach 4	Mach 5	Mach 6	Mach 7	Mach 8	Mach 9
St_{CFD}	0.56 ●	0.54 ●	0.45 ●	0.41 ●	0.38 ●	0.28 ●	0.32 ●	0.29 ●
St_{model}	0.57 ○	0.51 ○	0.43 ○	0.39 ○	0.384 ○	0.264 ○	0.287 ○	0.299 ○
% error, CFD/model	1.79%	5.55%	4.44%	4.87%	1.05%	5.71%	10.3%	3.01%
$St_{\text{Heller-Bliss}}$	0.57	0.51	0.49	0.48	0.478	0.474	0.471	0.469
%, CFD/Heller-Bliss	1.79%	5.88%	8.16%	14.6%	20.5%	40.93%	32.06%	38.17%

5 Acknowledgements

Research was sponsored by the DEVCOM Army Research Laboratory and was accomplished in-part under Cooperative Agreement Number W911NF-24-2-0152 and W911NF-23-2-0026. Luis Bravo was supported by the 6.1 program in propulsion sciences. The authors gratefully acknowledge the High-Performance Computing Modernization Program (HPCMP) resources and support provided by the Department of Defense Supercomputing Resource Center (DSRC) as part of the 2022 Frontier Project, Large-Scale Integrated Simulations of Transient Aerothermodynamics in Gas Turbine Engines.

The views and conclusions contained in this document are those of the authors and should not be interpreted as representing the official policies, either expressed or implied, of the DEVCOM Army Research Laboratory or the U.S. Government. The U.S. Government is authorized to reproduce and distribute reprints for Government purposes notwithstanding any copyright notation herein.

References

DECHANT, LAWRENCE 2019 A cavity depth sensitized rossiter mode formula. *Applied Mathematics and Computation* **347**, 143–148.

GIBBONS, NICHOLAS N, DAMM, KYLE A, JACOBS, PETER A & GOLLAN, ROWAN J 2023 Eilmer: An open-source multi-physics hypersonic flow solver. *Computer Physics Communications* **282**, 108551.

GUPTA, ROOP N, YOS, JERROLD M, THOMPSON, RICHARD A & LEE, KAM-PUI 1990 A review of reaction rates and thermodynamic and transport properties for an 11-species air model for chemical and thermal nonequilibrium calculations to 30000 k .

HELLER, H & BLISS, D 1975 The physical mechanism of flow-induced pressure fluctuations in cavities and concepts for their suppression. In *2nd Aeroacoustics conference*, p. 491.

REDDING, JEREMY, GAMERTSFELDER, JACOB, BRAVO, LUIS & KHARE, PRASHANT 2023 Thermochemical non-equilibrium hypersonic flow over a rectangular cavity embedded on a compression ramp. *Physics of Fluids* **35** (12).

REDDING, JEREMY, KHARE, PRASHANT & BRAVO, LUIS 2025 Vortex behavior in a dynamically moving hypersonic cavity. *Physics of Fluids* **37** (5).

ROCKWELL, D & NAUDASCHER, ET 1978 Self-sustaining oscillations of flow past cavities. *Journal of Fluids Engineering* **100** (2), 152–165.

ROSSITER, JE 1964 Wind-tunnel experiments on the flow over rectangular cavities at subsonic and transonic speeds .

VINCENTI, WALTER G, KRUGER JR, CHARLES H & TEICHMANN, T 1966 Introduction to physical gas dynamics.